

Cite this: *Nanoscale*, 2011, **3**, 2294

www.rsc.org/nanoscale

PAPER

## Photoluminescence and conductivity studies of anthracene-functionalized ruthenium nanoparticles<sup>†</sup>

Wei Chen,<sup>‡</sup> Sulolit Pradhan<sup>§</sup> and Shaowei Chen<sup>\*</sup>

Received 11th February 2011, Accepted 13th March 2011

DOI: 10.1039/c1nr10158g

Carbene-stabilized ruthenium nanoparticles were functionalized with anthryl moieties by olefin metathesis reactions with 9-vinylanthracene, at a surface concentration of about 19.7%, as estimated by <sup>1</sup>H NMR spectroscopic measurements. Because of the conjugated metal–ligand interfacial bonding interactions, UV-vis measurements of the resulting nanoparticles showed a new broad absorption band centered at 612 nm, in addition to the peaks observed with monomeric vinylanthracene. FTIR measurements depicted apparent red-shifts of the aromatic vibrational stretches as compared to those of the monomeric vinylanthracene, suggestive of decreasing bonding order of the aromatic moieties as a result of extended conjugation between the particle-bound anthracene groups. Photoluminescence measurements confirmed the notion that effective intraparticle charge delocalization occurred by virtue of the conjugated metal–ligand interfacial bonding interactions, with apparent red-shifts of the excitation peaks and blue-shifts of the emission features, as compared to those of the monomeric vinylanthracene. The diminishment of the Stokes shift was, at least in part, attributed to the different chemical environments surrounding the anthryl moieties on the nanoparticle surface. Electronic conductivity measurements showed that because of the conjugated Ru=C π bonds, the activation energy for interparticle charge transport was about one order of magnitude lower than that observed with particles passivated by alkanethiolates. Additionally, whereas the original carbene-stabilized nanoparticles exhibited a semiconductor–metal transition within the temperature range of 100 to 320 K, anthracene-functionalized nanoparticles displayed apparent semiconducting behaviors with the ensemble conductivity increasing monotonically with temperature, most likely due to the disordering within the nanoparticle solids that arose from the different structures of the carbene ligands and anthryl moieties. These studies indicate that anthracene functionalization may be exploited as an effective route towards the manipulation of nanoparticle optoelectronic properties.

### Introduction

Nanometre-sized metal particles have been attracting extensive research interest primarily because of their unique chemical and physical properties that are vastly different from those of their atomic and bulk forms<sup>1</sup> and thus may be exploited as unique functional building blocks for a wide range of nanotechnological applications, such as nanoscale optoelectronic devices,<sup>2–4</sup>

chemical sensors/biosensors<sup>5–7</sup> and (electro/photo)catalysts.<sup>8–11</sup> Because of the composite characters of the nanoparticle structures, it has been well-documented that the materials properties can be readily manipulated by the chemical nature of the metal cores as well as the organic protecting ligands.<sup>12–14</sup> Recently, it has also been demonstrated that the nanoparticle optical and electronic properties can be further controlled by the metal–ligand interfacial bonding interactions, thanks to the advances in nanoparticle surface functionalization where nanoparticles can be stabilized by metal–carbon covalent bonds, in contrast to those with conventional metal–thiolate chemical linkages.<sup>15–24</sup> Of these, metal nanoparticles stabilized by carbene fragments by virtue of metal–carbon π bonds have been found to exhibit apparent intraparticle charge delocalization between the particle-bound functional moieties, which has been manifested, for instance, by the nanoparticle-mediated intervalence transfer between ferrocenyl moieties bound on the ruthenium nanoparticle surface<sup>19</sup> as well as dimer-like photoluminescence characteristics of pyrene-functionalized nanoparticles.<sup>21,22</sup> The

Department of Chemistry and Biochemistry, University of California, 1156 High Street, Santa Cruz, California, 95064, USA. E-mail: shaowei@ucsc.edu

<sup>†</sup> Electronic supplementary information (ESI) available: Deconvolution of fluorescence spectra of monomeric 9-vinylanthracene and Ru=VAN nanoparticles, and Arrhenius plots of the Ru=C8 and Ru=VAN nanoparticle electronic conductivity. See DOI: 10.1039/c1nr10158g

<sup>‡</sup> Present address: State Key Laboratory of Electroanalytical Chemistry, Changchun Institute of Applied Chemistry, Chinese Academy of Sciences, Changchun, Jilin 130022, China.

<sup>§</sup> Present address: National Renewal Energy Laboratory, Golden, Colorado 80401, USA.

functionalization is made possible by the unique olefin metathesis reactions of the carbene-stabilized nanoparticles with functional vinyl derivatives.<sup>15</sup>

In the present study, we extend the research to anthracene-functionalized ruthenium nanoparticles, primarily motivated by the unique photoluminescence characteristics that arise from the anthryl moieties as well as by the manipulation of the nanoparticle ensemble conductivity by anthracene functionalization. Anthracene derivatives have been well-known for their unique scintillation characteristics,<sup>25,26</sup> where the strong and highly sensitive luminescence may be exploited for diverse applications in, for instance, lasers, phosphors and light-emitting devices.<sup>27,28</sup> Towards this end, anthracene-based functional molecules have been prepared and examined extensively as possible photoluminescence or electroluminescence materials.<sup>29–32</sup> However, at relatively high concentrations, the close proximity of anthryl moieties may lead to the formation of excimers that exhibit markedly different photoluminescence characteristics as compared to those of the monomeric forms. In fact, three types of excimers with slightly different geometric configurations have been identified. The first excimer is relatively stable, with the two anthryl units overlapping at an angle of 55° to each other. This type of excimers features a short excited state lifetime (<10 ns) with an emission maximum close to 470 nm.<sup>33</sup> The second one exhibits a “sandwich” structure with symmetrical  $\pi$ -stacking of the two anthryl units, longer lifetimes at lower temperatures and an emission maximum at 560 nm.<sup>33</sup> The third type of anthracene excimers involves the formation of a T-shaped structure with an emission maximum at 510 nm and an excited state lifetime of ~20 ns.<sup>34</sup> One can see that (i) stable excimers may be formed only when the anthryl moieties are in optimal orientation and separation and (ii) regardless of the geometric configurations, the excimers all exhibit an apparent red-shift of the photoluminescence emission as compared to that of monomeric anthracene. Therefore, an immediate question arises, will excimers of anthracene be formed when the anthryl moieties are incorporated onto the nanoparticle surface? Whereas the anthryl groups most likely are situated in close proximity, the rigid chemical environment may render it difficult to achieve an optimal orientation for excimer formation. Thus, it is imperative to examine the optical properties of anthracene-functionalized nanoparticles before they may be used as novel building blocks for device fabrication.

In addition, recently we demonstrated that transition-metal nanoparticles passivated by metal–carbon covalent bonds exhibited a markedly enhanced electronic conductivity as compared to the mercapto-stabilized counterparts, which was interpreted on the basis of the low interfacial contact resistance that allowed effective spilling of core electrons into the organic layers.<sup>16–18</sup> Yet, most of these earlier studies are focused on metal nanoparticles stabilized by metal–carbon single bonds. The carbene-stabilized nanoparticles offer a unique platform where the impacts of metal–carbene  $\pi$  bonds on nanoparticle charge transport can be evaluated. In addition, because of intraparticle charge delocalization, the dynamics of interparticle charge transfer may be further regulated by the functional moieties residing on the nanoparticle surface.

Herein, anthracene-functionalized ruthenium nanoparticles were prepared by olefin metathesis reactions of carbene-

stabilized ruthenium nanoparticles with 9-vinylanthracene. Despite the close proximity of the anthryl moieties on the nanoparticle surface, no formation of excimers was observed, as manifested in photoluminescence measurements, most probably because of the rigid ligand shell surrounding the anthracene groups that rendered it difficult to achieve an optimal configuration for excimer formation. However, because of the conjugated metal–ligand interfacial bonding interactions, the particle-bound anthracene moieties behaved analogously to bianthracene derivatives with a conjugated chemical linker, suggesting effective intraparticle charge delocalization. Since the nanoparticles can serve as a nanoscale structural scaffold for chemical decorations with multiple functional moieties, the unique photoluminescence properties of anthracene-functionalized nanoparticles may be further manipulated by intraparticle electronic communication with other functional moieties. Furthermore, electronic conductivity measurements were carried out and it was found that the Ru=C  $\pi$  bonds led to enhanced interparticle charge transport whereas the incorporation of anthryl moieties onto the nanoparticle surface produced structural disordering within the nanoparticle solid ensembles that led to diminishment of the interparticle charge transport.

## Experimental section

### Chemicals

Ruthenium chloride (RuCl<sub>3</sub>, 99+%, Acros), 1,2-propanediol (Acros), sodium acetate trihydrate (NaAc·3H<sub>2</sub>O, MC&B), 9-vinylanthracene (98%, Acros), 1,1,1,3,3,3-hexamethyldisilazane (98%, Acros), octyl acetate (99+%, Aldrich), *n*-butyllithium (2.5 M in hexanes, Aldrich), and 2,2,2-trifluoroethyl trifluoroacetate (99%, Aldrich), and extra dry *N,N*-dimethylformamide (DMF, 99.8%, Aldrich) were used as received. All solvents were obtained from typical commercial sources and used without further treatment. Water was supplied by a Barnstead Nanopure water system (18.3 M $\Omega$  cm).

### Carbene-stabilized ruthenium nanoparticles

The preparation of ruthenium nanoparticles passivated by carbene fragments has been detailed previously.<sup>15</sup> In brief, octyl diazoacetate (ODA) was first synthesized by following a modified literature procedure and Ru nanoparticles were produced by thermolytic reduction of ruthenium chloride in 1,2-propanediol. Experimentally, 0.65 mmol of RuCl<sub>3</sub> and 2 mmol of NaAc were dissolved in 200 mL of 1,2-propanediol. The mixed solution was heated to 165 °C for 15 min under vigorous stirring. After the colloid solution was cooled to room temperature, octyl diazoacetate (ODA) dissolved in toluene with three-fold molar excess as compared to Ru was added into the solution under magnetic stirring overnight. It was found that ruthenium nanoparticles were transferred to the toluene phase because of the strong affinity of the diazo moieties to the ruthenium surface by the formation of Ru=carbene  $\pi$  bonds. A copious amount of methanol was then used to remove excessive ligands, affording purified Ru nanoparticles. The resulting purified nanoparticles were denoted as Ru=C8, which exhibited a core diameter of 2.12 ± 0.72 nm as determined by transmission electron microscopy (TEM) measurements.<sup>15</sup>

## Anthracene-functionalized ruthenium nanoparticles

The Ru=C8 particles obtained above were then functionalized with anthryl moieties by olefin metathesis reactions with 9-vinylanthracene (Scheme 1). In a typical reaction, Ru=C8 and 9-vinylanthracene (the molar ratio of vinylanthracene to the particle-bound carbene ligands was *ca.* 3 : 1) were co-dissolved in dichloromethane (DCM) under magnetic stirring for 3 days. Excessive ethanol was added to the solution to precipitate the nanoparticles, which were separated by centrifugation and washed extensively by ethanol to remove excessive vinylanthracene and displaced ligands. The resulting particles were referred to as Ru=VAN.

## Spectroscopies

The surface coverage of the anthracene moieties was evaluated by using proton nuclear magnetic resonance (<sup>1</sup>H NMR) spectroscopy (Varian Unity 500 MHz). Experimentally, the metal cores of the Ru=VAN nanoparticles were dissolved by dilute potassium cyanide (KCN) and the organic components were collected by extraction with CD<sub>2</sub>Cl<sub>2</sub> for NMR measurements. UV-Vis spectroscopic studies were performed with an ATI Unicam UV4 spectrometer using a 1 cm quartz cuvette with a resolution of 2 nm. Photoluminescence characteristics were examined with a PTI fluorospectrometer, and infrared spectra were acquired with a Perkin Elmer Spectrum One FTIR spectrometer by drop casting the nanoparticle solution onto a KBr disk. The spectral resolution was 4 cm<sup>-1</sup>.

## Electronic conductivity

Conductivity measurements were carried out with solid films of the ruthenium nanoparticles (Ru=C8 or Ru=VAN) by drop casting a known amount of the respective particle solution onto an interdigitated array electrode (IDA, 25 pairs of gold fingers of 3 mm × 5 μm × 5 μm, from Abtech).<sup>16–18</sup> Typically, 5 μL of a particle solution (at a concentration of 5.00 mg mL<sup>-1</sup> in DCM for Ru=C8 and in DMF for Ru=VAN) was drop cast onto an IDA electrode surface where the gaps between the IDA fingers were all filled up, and the particle films were then subject to vapor annealing with the respective solvent for 30 min. Current–potential (*I–V*) profiles were then acquired at the potential sweep rate of 20 mV s<sup>-1</sup> in vacuum (Cryogenic Equipment, Janis Co.) with a CHI 710 Electrochemical Workstation within the temperature range of 100 to 320 K (Lakeshore 331 Temperature Controller). The ensemble conductivity ( $\sigma$ ) was evaluated by the

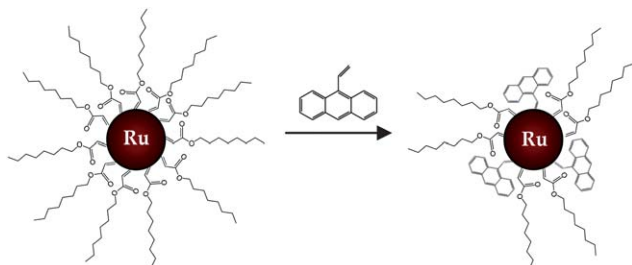
equation  $\sigma = \left(\frac{1}{49R}\right)\left(\frac{S}{L}\right)$ , where *R* is the ensemble resistance calculated from the slope of the *I–V* curves, *L* is the IDA electrode interfinger gap (5 μm) and *S* is the film cross-section area approximated by (finger height, 5 μm) × (finger length, 3 mm). The constant (49) reflects that there are totally 49 junctions which are in parallel within the IDA chip.

## Results and discussion

### Structural characterizations

The surface coverage of the anthryl moieties bound onto the Ru nanoparticle surface was first quantified by <sup>1</sup>H NMR spectroscopic measurements. Fig. 1 depicts the <sup>1</sup>H NMR spectra of (A) Ru=VAN nanoparticles after the metal core was dissolved by dilute KCN and (B) monomeric 9-vinylanthracene. The peak at  $\delta = 0.9$  ppm in (A) can be ascribed to the methyl proton of the carbene ligands, and the peaks at 7.5, 8.0, and 8.3 ppm in both curves (A) and (B) to the aromatic protons of the anthracene rings. However, the peaks at 5.6 and 6.0 ppm from the vinyl protons of vinylanthracene monomers (curve B) disappeared in Ru=VAN (curve A), which is consistent with the cleavage of the vinyl C=C double bond as a result of olefin metathesis reactions with the Ru=C8 nanoparticles (Scheme 1). The appearance of methyl protons with Ru=VAN indicates that not all the original carbene ligands were replaced by the vinylanthracene molecules. On the basis of the ratio of the integrated peak areas from the methyl protons and the aromatic protons of the anthracene rings, the surface coverage of the anthryl moieties on the Ru nanoparticles was estimated to be 19.7%.

The incorporation of anthryl moieties into the particle protecting monolayer was also confirmed by Fourier-transformed infrared (FTIR) spectroscopic measurements (Fig. 2). For instance, the strong peaks at ~734 cm<sup>-1</sup> and 884 cm<sup>-1</sup> can be assigned to the out-of-plane deformation of aromatic C–H of the carbon quartets at the ends and of the central carbons of the anthryl moieties, respectively.<sup>35</sup> These two bands are well-defined in both the Ru=VAN nanoparticles and vinylanthracene monomers. However, with reference to the 884 cm<sup>-1</sup> band, the 734 cm<sup>-1</sup> band was substantially weaker for the Ru=VAN nanoparticles than for the vinylanthracene monomers, which might be accounted for by the steric hindrance arising from the enclosure of the anthryl moieties within the nanoparticle



**Scheme 1** Olefin metathesis reaction of carbene-stabilized Ru nanoparticles with 9-vinylanthracene

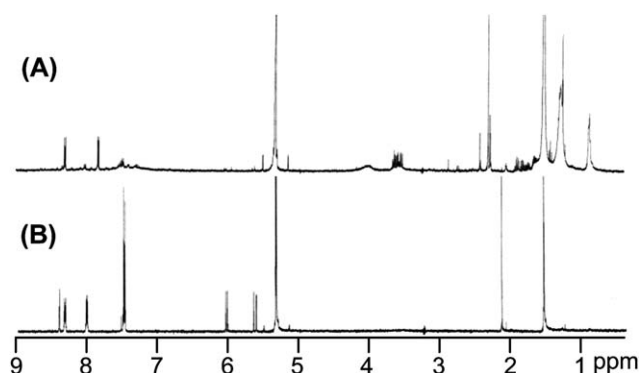


**Fig. 1** <sup>1</sup>H NMR spectra of (A) Ru=VAN nanoparticles and (B) 9-vinylanthracene monomer with CD<sub>2</sub>Cl<sub>2</sub> as the solvent.

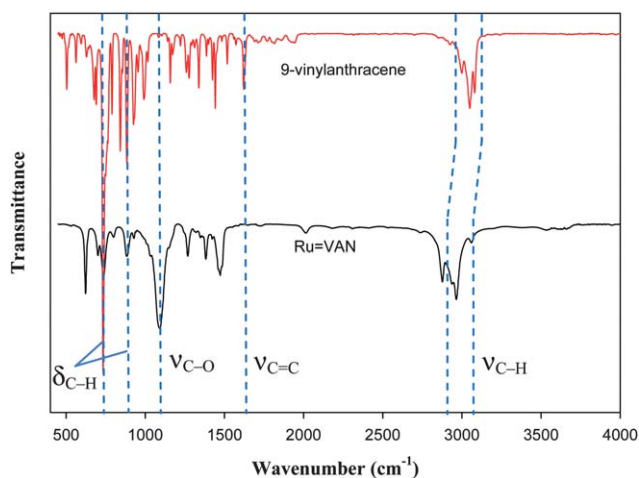


**Fig. 2** FTIR spectra of (top curve) 9-vinylanthracene and (bottom curve) Ru=VAN nanoparticles.

protecting layer (Scheme 1). In fact, because of this, whereas the anthracene skeletal vibration at  $954\text{ cm}^{-1}$  can be identified with the monomeric vinylanthracene, its intensity diminished drastically with the Ru=VAN nanoparticles. Additionally, the (aromatic)  $\text{=C-H}$  vibrational stretches at  $3077$ ,  $3049$  and  $2997\text{ cm}^{-1}$  for monomeric vinylanthracene were found to exhibit a marked red-shift to  $3059$ ,  $2965$ , and  $2934\text{ cm}^{-1}$  when the anthryl moieties were incorporated onto the Ru particle surface, which suggests a decrease of the bonding order within the anthryl moieties. This is analogous to previous observations with Ru=C8 nanoparticles<sup>15</sup> and ruthenium-carbene complexes,<sup>36</sup> where the red-shift was accounted for by intraparticle/intramolecular charge delocalization that arose from the conjugated Ru=C  $\pi$  bond. Note that the Ru=VAN nanoparticles also exhibited a peak at  $2871\text{ cm}^{-1}$  and another prominent one at  $1091\text{ cm}^{-1}$ , which may be assigned to the methylene C-H and C-O vibrational bands of the original carbene fragments, respectively. Furthermore, the vinyl (C=C) vibrational band observed at  $1630\text{ cm}^{-1}$  with the vinylanthracene monomers disappeared when the ligands underwent metathesis reactions with Ru=C8 nanoparticles and were bound to the particle surface, consistent with the cleavage of the C=C double bonds and the formation of Ru=C  $\pi$  bonds.

### Optical characteristics

The functionalization of the Ru nanoparticles by anthryl moieties was further manifested in optical absorption measurements. Fig. 3 depicts the UV-vis absorption spectra of Ru=C8, Ru=VAN nanoparticles, and monomeric 9-vinylanthracene. It can be seen that the absorption profiles of Ru=C8 (red curve) and Ru=VAN (green curve) nanoparticles are very similar, both consistent with the Mie characters of nanosized metal particles. However, subtraction of the Ru=C8 spectrum from that of Ru=VAN yields a profile (blue curve) that features three apparent absorption peaks at  $352$ ,  $370$  and  $390\text{ nm}$ , which are consistent with those observed with monomeric vinylanthracene (black curve). This again indicates the successful incorporation of the anthryl moieties onto the nanoparticle surface, in

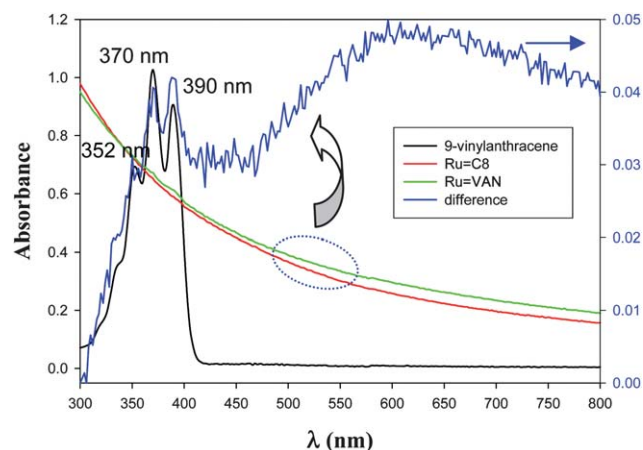


**Fig. 3** UV-visible absorption spectra of 9-vinylanthracene monomers and the Ru particles before (Ru=C8) and after (Ru=VAN) exchange reactions. The difference of the last two spectra was also included. Both particle concentrations were  $0.1\text{ mg mL}^{-1}$  in DMF. For the anthracene monomer, the concentration was  $0.1\text{ mM}$  in DMF.

agreement with the  $^1\text{H NMR}$  and FTIR results presented above (Fig. 1 and 2). In addition, a new broad absorption peak can be found at  $612\text{ nm}$ , signifying the emergence of new electronic energy states that most likely arose from intraparticle charge delocalization between the anthryl moieties as a consequence of the conjugated Ru=C  $\pi$  bonds, akin to that observed previously with pyrene-functionalized nanoparticles.<sup>21,22</sup>

In fact, the photoluminescence properties of the particle-bound anthryl moieties exhibited an apparent deviation from those of monomeric vinylanthracene. Fig. 4 shows the excitation (solid curves) and emission (dashed curves) spectra of 9-vinylanthracene and Ru=VAN nanoparticles in DMF. It can be seen that, in comparison to the featureless responses of Ru=C8 nanoparticles (blue curve), monomeric vinylanthracene (black curve) and Ru=VAN nanoparticles (red curve) both exhibit four well-defined excitation peaks that are in agreement with their respective UV-vis absorption profiles (Fig. 3), vinylanthracene

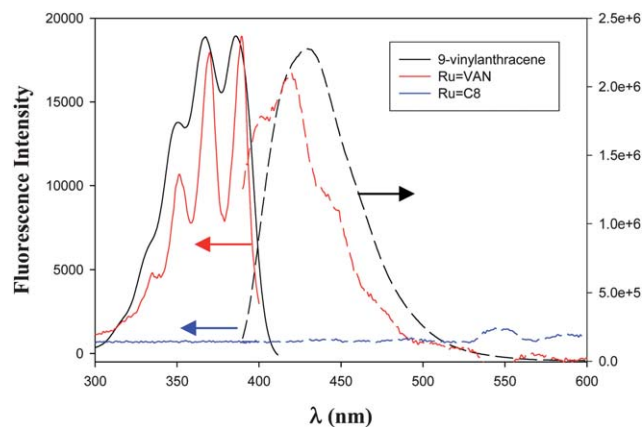


**Fig. 4** Excitation and emission spectra of 9-vinylanthracene monomers, Ru=C8, and Ru=VAN nanoparticles. The excitation wavelength was set at  $370\text{ nm}$  in both measurements. The solutions were the same as those in Fig. 3. Note that the left y axis is for the two nanoparticle samples whereas the right one for 9-vinylanthracene.

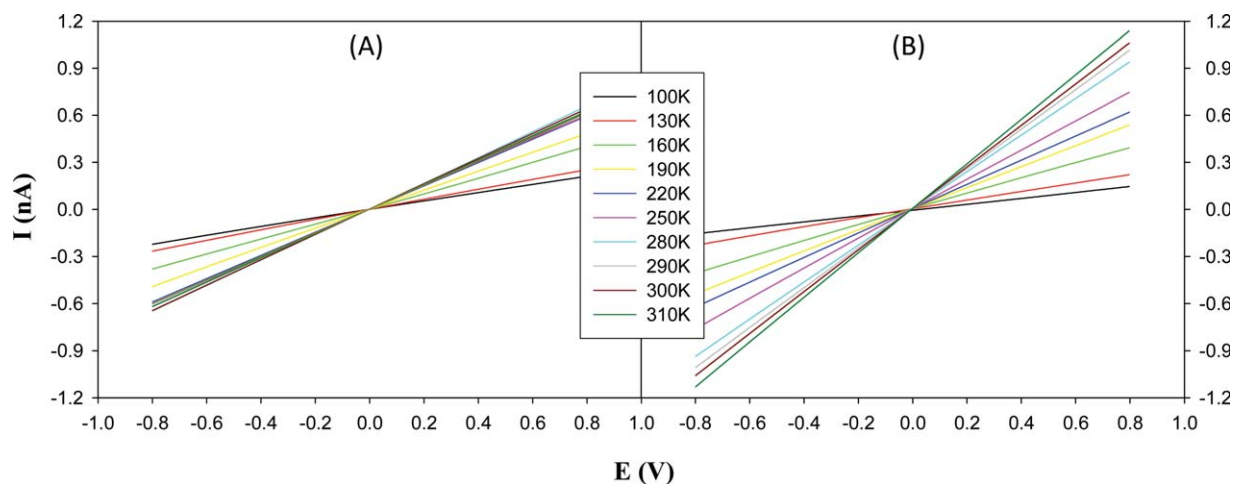


**Fig. 5** Current–potential ( $I$ – $V$ ) profiles of solid films of (A) Ru=C8 and (B) Ru=VAN nanoparticles at different temperatures (shown as figure legends). Potential scan rate was  $20 \text{ mV s}^{-1}$ .

(332, 350, 368, and 386 nm) and Ru=VAN (335, 351, 370, and 390 nm). The small red-shift of the latter might be, again, ascribed to the extended conjugation between the particle-bound anthryl moieties by virtue of the Ru=carbene  $\pi$  interfacial linkages.<sup>21,22</sup> A more significant difference can be seen in the emission spectra (at the same excitation wavelength of 370 nm), where peak deconvolution yields three major emission bands for both samples (Fig. S1†), with an apparent blue-shift observed with Ru=VAN (396, 415, and 440 nm) in comparison with vinylanthracene (411, 434, and 466 nm). There are at least three aspects that warrant attention here. First, the slight red-shift of the Ru=VAN excitation peaks and the lack of apparent emission at longer wavelengths ( $\geq 500 \text{ nm}$ ) strongly suggests that no excimer was formed for the particle-bound anthryl moieties.<sup>33,34,37</sup> Second, the decrease of Stokes shift observed with the Ru=VAN nanoparticles as compared to that of monomeric vinylanthracene might be accounted for, at least in part, by the rigid chemical environment within which the anthryl moieties were embedded (Scheme 1). As the translational and rotational movements of the anthryl moieties were impeded on the particle surface, the formation of excimers became energetically and sterically unfavorable and thus no apparent emission was observed in the long wavelength range. In addition, with the tightly packed ligand layers on the particle surface, it is anticipated that geometrical distortions of the molecules that might serve as trap states for efficient energy transfer would be minimal.<sup>38</sup> Third, it should be noted that the emission characteristics of Ru=VAN are very similar to those of bianthracene. For instance, 9,9'-bianthracene has been found to exhibit two prominent emission peaks at 395 and 419 nm in butyl acetate (a chemical environment that is analogous to that experienced by anthryl moieties on the nanoparticle surface protecting layer, Scheme 1).<sup>39</sup> This observation further supports the notion that effective intraparticle charge delocalization occurred between the particle-bound anthracene moieties as a result of conjugated Ru=C interfacial linkages. Also, as bianthracene exhibits apparent solvatochromic behaviors where the center of the emission band red-shifts markedly with increasing solvent polarity (e.g., in DMF, the emission center moved to 454–458 nm),<sup>39</sup> additional contributions to the diminishment of

the Stokes shift observed with Ru=VAN as compared to that of monomeric vinylanthracene might arise from the decrease of effective dielectric constant of the chemical environment surrounding the anthracene moieties.

### Electronic conductivity

The incorporation of anthryl moieties into the nanoparticle surface-protecting layer also led to an apparent variation of the nanoparticle electronic conductivity. Fig. 5 depicts the current–potential ( $I$ – $V$ ) profiles of solid films of (A) Ru=C8 and (B) Ru=VAN nanoparticles within the temperature range of 100 to 320 K. It can be seen that both samples exhibited linear (ohmic)  $I$ – $V$  characteristics, analogous to earlier studies of monolayer-protected nanoparticle molecules,<sup>40–44</sup> which were primarily accounted for by electron hopping between neighboring nanoparticles in the solid films where the organic protecting layer served as the tunneling barrier. However, the two nanoparticles exhibited markedly different temperature-dependence of the ensemble conductivity, as highlighted in Fig. 6. One can see that for Ru=C8 nanoparticles, at temperatures below 280 K, the ensemble conductivity increases with increasing temperature,

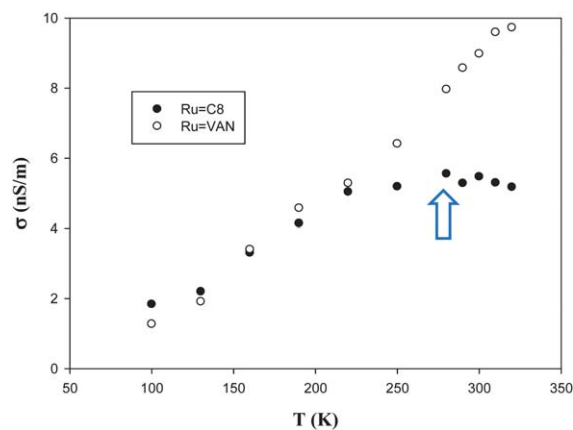


**Fig. 6** Variation of the nanoparticle conductivity with temperature. Data are acquired from Fig. 5. Arrow highlights the semiconductor–metal transition of the Ru=C8 nanoparticles.

suggestive of semiconducting characteristics due to the composite nature of the nanoparticles; whereas at higher temperatures (280 to 320 K), the particle conductivity actually decreased slightly with increasing temperature, a behavior that is anticipated of metallic materials. In other words, within the temperature range of 100 to 320 K, the electronic conductivity of Ru=C8 nanoparticles displayed a clear semiconductor–metal transition. Such a phenomenon has also been observed with solid films of palladium nanoparticles passivated by aryl fragments (with the formation of Pd–C covalent bonds) and interpreted by the Mott's model for metal–insulator transition.<sup>18</sup> In essence, the metal–carbon interfacial covalent linkage led to the extended spilling of core electrons into the organic protecting matrix and thus enhanced charge transport through the nanoparticle solids. Nonetheless, in comparison to the aliphatic structure of the surface protecting ligands of Pd–C nanoparticles,<sup>18</sup> the (polarized) ester moiety within the carbene ligands (Scheme 1) most likely limited the through-bond charge transport, as reflected by the higher transition temperature (~280 K, highlighted by the arrow in Fig. 6) observed here with the Ru=C8 nanoparticles than that (~180 K) for the Pd–C nanoparticle.<sup>18</sup>

In contrast, within the entire range of temperature under study (100 to 320 K), Ru=VAN nanoparticles exhibited a monotonic increase of ensemble conductivity with temperature. The lack of metallic characters at high temperatures is likely due to the disordering within the nanoparticle films that arose from the different molecular structures of the carbene fragments and the anthryl ligands (Scheme 1), as it has been known that disordering within the nanoparticle ensembles diminished the overlap of the electronic wavefunctions between neighboring nanoparticles.<sup>45</sup>

Notably, within the temperature range of 100 to 280 K, Ru=C8 and Ru=VAN nanoparticles exhibited highly comparable electronic conductivity, suggesting that the energetic barrier for interparticle charge transport was due to the carbene ligands. Furthermore, both nanoparticle samples showed apparent Arrhenius behaviors (Fig. S2†), suggesting that the interparticle charge transport was most likely dictated by the thermal activation mechanism. Linear regressions show that the activation energy ( $E_a$ ) for interparticle charge transport is in fact very close, at 9.8 and 11.5 meV, respectively. It should be noted that these values are at least one order of magnitude lower than that observed for alkanethiolate-passivated nanoparticles of similar core sizes.<sup>46</sup> This may be ascribed to the conjugated Ru=C interfacial bonding interactions that facilitated extended spilling of core electrons into the organic matrix, leading to the diminishment of the energetic barrier for interparticle charge transport.

## Concluding remarks

Anthracene-functionalized ruthenium nanoparticles were prepared by olefin metathesis reactions of carbene-stabilized nanoparticles with 9-vinylanthracene. The surface coverage of the anthryl moieties was evaluated to be 19.7% by <sup>1</sup>H NMR measurements. Because of the conjugated Ru=C  $\pi$  bonds, effective intraparticle charge delocalization occurred between the particle-bound anthryl moieties, and the particle-bound anthryl moieties behaved analogously to bianthracene derivatives, as manifested in FTIR, UV-vis and photoluminescence

spectroscopic measurements. In addition, whereas the electronic conductivity of the original carbene-stabilized nanoparticles exhibited a clear semiconductor–metal transition at around 280 K, the anthracene-functionalized counterparts displayed apparent semiconducting behaviors within the same temperature range of 100 to 320 K. The discrepancy was ascribed to the disordering within the nanoparticle solids that arose from the different chemical structures of the original carbene ligands and the anthryl moieties. The results from this study strongly suggest that anthracene functionalization might be exploited for the ready manipulation of the nanoparticle optoelectronic properties.

On-going work is focused on the mechanistic correlation between the nanoparticle optical and electronic properties and the results will be reported in due course.

## Acknowledgements

This work was supported in part by the National Science Foundation (CHE-0718190/CHE-1012258, and CHE-0832605) and the ACS–Petroleum Research Fund (49137-ND10).

## Notes and references

- G. Schmid, *Chem. Rev.*, 1992, **92**, 1709.
- R. P. Andres, J. D. Bielefeld, J. I. Henderson, D. B. Janes, V. R. Kolagunta, C. P. Kubiak, W. J. Mahoney and R. G. Osifchin, *Science*, 1996, **273**, 1690.
- S. W. Chen, R. S. Ingram, M. J. Hostetler, J. J. Pietron, R. W. Murray, T. G. Schaaff, J. T. Khoury, M. M. Alvarez and R. L. Whetten, *Science*, 1998, **280**, 2098.
- C. A. Berven, L. Clarke, J. L. Mooster, M. N. Wybourne and J. E. Hutchison, *Adv. Mater.*, 2001, **13**, 109.
- P. Schwerdtfeger, *Angew. Chem., Int. Ed.*, 2003, **42**, 1892.
- T. Huang and R. W. Murray, *J. Phys. Chem. B*, 2001, **105**, 12498.
- S. R. Emery, W. E. Haskins and S. M. Nie, *J. Am. Chem. Soc.*, 1998, **120**, 8009.
- C. Mohr, H. Hofmeister, J. Radnik and P. Claus, *J. Am. Chem. Soc.*, 2003, **125**, 1905.
- L. N. Lewis, *Chem. Rev.*, 1993, **93**, 2693.
- H. Tsunoyama, H. Sakurai, Y. Negishi and T. Tsukuda, *J. Am. Chem. Soc.*, 2005, **127**, 9374.
- W. Chen and S. W. Chen, *Angew. Chem., Int. Ed.*, 2009, **48**, 4386.
- R. L. Whetten, M. N. Shafiqullin, J. T. Khoury, T. G. Schaaff, I. Vezmar, M. M. Alvarez and A. Wilkinson, *Acc. Chem. Res.*, 1999, **32**, 397.
- R. Shenhar and V. M. Rotello, *Acc. Chem. Res.*, 2003, **36**, 549.
- R. W. Murray, *Chem. Rev.*, 2008, **108**, 2688.
- W. Chen, J. R. Davies, D. Ghosh, M. C. Tong, J. P. Konopelski and S. W. Chen, *Chem. Mater.*, 2006, **18**, 5253.
- D. Ghosh, S. Pradhan, W. Chen and S. W. Chen, *Chem. Mater.*, 2008, **20**, 1248.
- D. Ghosh and S. W. Chen, *Chem. Phys. Lett.*, 2008, **465**, 115.
- D. Ghosh and S. W. Chen, *J. Mater. Chem.*, 2008, **18**, 755.
- W. Chen, S. W. Chen, F. Z. Ding, H. B. Wang, L. E. Brown and J. P. Konopelski, *J. Am. Chem. Soc.*, 2008, **130**, 12156.
- W. Chen, L. E. Brown, J. P. Konopelski and S. W. Chen, *Chem. Phys. Lett.*, 2009, **471**, 283.
- W. Chen, N. B. Zuckerman, J. W. Lewis, J. P. Konopelski and S. W. Chen, *J. Phys. Chem. C*, 2009, **113**, 16988.
- W. Chen, N. B. Zuckerman, J. P. Konopelski and S. W. Chen, *Anal. Chem.*, 2010, **82**, 461.
- W. Chen, N. B. Zuckerman, X. W. Kang, D. Ghosh, J. P. Konopelski and S. W. Chen, *J. Phys. Chem. C*, 2010, **114**, 18146.
- X. W. Kang and S. W. Chen, *Angew. Chem., Int. Ed.*, 2010, **49**, 9496.
- P. E. Gibbons, D. C. Northrop and O. Simpson, *Proc. Phys. Soc. Lond.*, 1962, **79**, 373.
- M. Imoto and T. Nakaya, *Bull. Chem. Soc. Jpn.*, 1963, **36**, 785.

- 27 Y. Y. Lyu, J. Kwak, O. Kwon, S. H. Lee, D. Kim, C. Lee and K. Char, *Adv. Mater.*, 2008, **20**, 2720.
- 28 S. G. Turrion, D. Olmos, N. Ekizoglou and J. Gonzalez-Benito, *Polymer*, 2005, **46**, 4023.
- 29 K. Danel, T. H. Huang, J. T. Lin, Y. T. Tao and C. H. Chuen, *Chem. Mater.*, 2002, **14**, 3860.
- 30 B. X. Mi, Z. Q. Gao, M. W. Liu, K. Y. Chan, H. L. Kwong, N. B. Wong, C. S. Lee, L. S. Hung and S. T. Lee, *J. Mater. Chem.*, 2002, **12**, 1307.
- 31 S. K. Kim, B. Yang, Y. I. Park, Y. G. Ma, J. Y. Lee, H. J. Kim and J. Park, *Org. Electron.*, 2009, **10**, 822.
- 32 J. F. Li, W. L. Chang, C. L. Tao, G. P. Ou and F. J. Zhang, *Chin. Phys. Lett.*, 2008, **25**, 4476.
- 33 L. S. Kaanumalle, C. L. D. Gibb, B. C. Gibb and V. Ramamurthy, *J. Am. Chem. Soc.*, 2005, **127**, 3674.
- 34 G. Q. Zhang, G. Q. Yang, S. Q. Wang, Q. Q. Chen and J. S. Ma, *Chem.-Eur. J.*, 2007, **13**, 3630.
- 35 A. C. Brieva, C. Jager, F. Huisken, L. Siller and Y. V. Butenko, *Carbon*, 2009, **47**, 2812.
- 36 I. Iwakura, H. Tanaka, T. Ikeno and T. Yamada, *Chem. Lett.*, 2004, **33**, 140.
- 37 J. B. Birks and J. B. Aladekomo, *Photochem. Photobiol.*, 1963, **2**, 415.
- 38 G. Biesmans, G. Verbeek, B. Verschuere, M. Vanderauweraer and F. C. Deschryver, *Thin Solid Films*, 1989, **169**, 127.
- 39 S. A. Tucker, J. M. Griffin, W. E. Acree, M. Zander and R. H. Mitchell, *Appl. Spectrosc.*, 1994, **48**, 458.
- 40 W. P. Wuefling and R. W. Murray, *J. Phys. Chem. B*, 2002, **106**, 3139.
- 41 L. Clarke, M. N. Wybourne, L. O. Brown, J. E. Hutchison, M. Yan, S. X. Cai and J. F. W. Keana, *Semicond. Sci. Technol.*, 1998, **13**, A111.
- 42 R. C. Doty, H. B. Yu, C. K. Shih and B. A. Korgel, *J. Phys. Chem. B*, 2001, **105**, 8291.
- 43 A. W. Snow and H. Wohltjen, *Chem. Mater.*, 1998, **10**, 947.
- 44 L. Y. Wang, X. J. Shi, N. N. Kariuki, M. Schadt, G. R. Wang, Q. Rendeng, J. Choi, J. Luo, S. Lu and C. J. Zhong, *J. Am. Chem. Soc.*, 2007, **129**, 2161.
- 45 F. Remacle and R. D. Levine, *J. Am. Chem. Soc.*, 2000, **122**, 4084.
- 46 S. Pradhan, J. Sun, F. J. Deng and S. W. Chen, *Adv. Mater.*, 2006, **18**, 3279.